NOTES AND CORRESPONDENCE

Interpretation of GPS Offsets from a Steady Course

MATTHEW DZIECIUCH AND WALTER MUNK

Scripps Institution of Oceanography, La Jolla, California

ANDREW FORBES

Commonwealth Scientific and Industrial Research Organization, Hobart, Tasmania, Australia

14 November 1991 and 22 April 1992

ABSTRACT

We have recorded time series of ship GPS (global positioning system) positions at about 10-s intervals under favorable satellite conditions. Errors are less than 10 m rms, as demonstrated by comparing the GPS acoustic-source positions with Doppler-inferred positions from a receiver site 9200 km away. Offsets from a steady course held for 20 miles are of the order of 100 m, and could be the result of orbital surface velocities associated with internal waves. We suggest that such GPS measurements, taken routinely while under way, might produce useful data concerning small-scale oceanographic processes.

1. Introduction

We suggest that a modern version of the ancient technique of *dead reckoning* might provide some useful data concerning small-scale ocean processes.

The Heard Island Feasibility Test (Munk and Forbes 1989) presented a unique opportunity for testing GPS (global positioning system) navigation under operational conditions (not dockside). Acoustic transmissions were made with an acoustic-source array suspended from the *Cory Chouest* while she was underway into the wind and swell at about 3 kt (sound speed is 3000 kt). For a 57-Hz CW transmission this yields a Doppler shift by $+0.057 \cos A$ Hz, where A is the angle between the local ray azimuth and the ship's course. The signal was recorded at fixed receiver sites (among others) on both coasts of North America. Doppler corrections (or rather time compressions for a signal of finite bandwidth) are required and routinely made by a very efficient scheme devised by Metzger (1983). Coherent processing requires that the offsets from a steady course be less than about a quarter acoustic wavelength (less than 6 m at 57 Hz). It is then important to know over what time interval a *constant* Doppler correction can be applied, given the irregularity in the ship's course and speed. Accordingly, we made a major attempt to keep track of the ship's position, taking advantage of the fact that GPS was on a war alert and its coarse acquisition (CA) code was not degraded in the usual manner.

2. An acoustic validation of GPS offsets

Figure 1 shows the situation for an acoustic run during 0600–0700 UTC 26 January 1991. The *Cory Chouest* was within the immediate vicinity of Heard Island. Winds were 25–30 kt from 285°T, and swells 15–18 ft from 315°T. Course was 300°T into the wind and swell at 3.1 kt. The upper panel of Fig. 1 shows the east and west components of position determined by GPS at about 10-s intervals. On this scale the GPS positions do not deviate perceptibly from a straight line. Offsets from the straight line in ship coordinates ξ (bow) and η (port) are shown on the center panel. In this case the forward (bow) component is larger (ξ_{rms} = 21.7 m, η_{rms} = 15.7 m), but this is not always so.

A third set of components is oriented relative to the acoustic ray direction. The azimuthal launch angle at Heard Island toward the receiver at Ascension Island is 267°T. The lower panel of Fig. 1 shows the corresponding offset $x(t)$. The *predicted* Ascension Doppler is then

$$\Delta f(t) = \frac{\dot{x}(t - \tau)}{C} f, \qquad (1)$$

where $\dot{x} = dx/dt$ is the instantaneous velocity component of the *Cory Chouest* in the direction 267°T, C is sound speed, τ = 6252 s is the acoustic travel time, and f = 57 Hz is the transmitted acoustic frequency.

Corresponding author address: Dr. Walter Munk, Institute of Geophysics and Planetary Physics, 0225 Scripps Institution of Oceanography, 9500 Gilman Dr., La Jolla, CA 92093-0225.

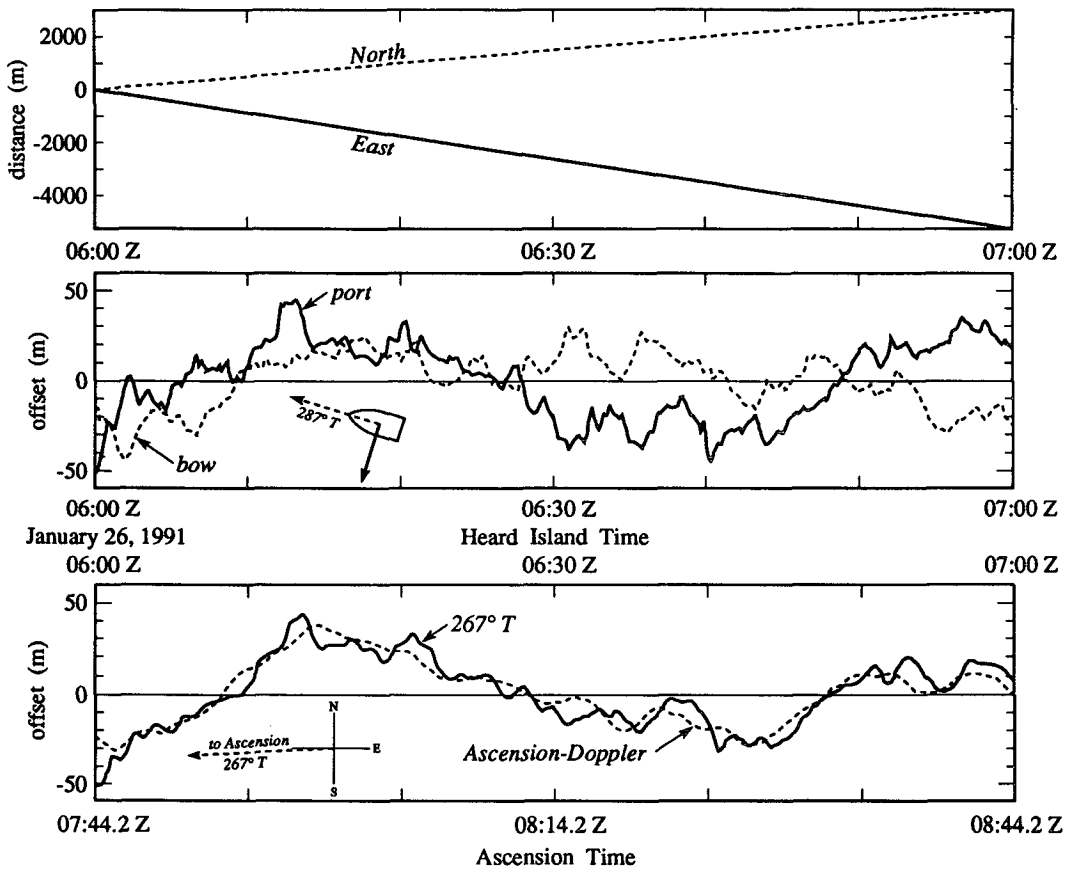

FIG. 1. Upper panel: East and west components of position determined by GPS as a function of time. The ship was on automatic pilot with propeller rpm and pitch set. On this scale, the GPS positions deviate imperceptibly from a straight line. Center panel: Offsets from the straight line. The rms components in ship coordinates are 21.7 and 15.7 m bow and port, respectively. Lower panel: Solid curve is the GPS component offset in the direction of 267°T (the launch angle of the refracted geodesic toward Ascension Island). Dashed curve is inferred from the integrated Doppler measured at Ascension Island, with a time shift of 6252 s to allow for acoustic transmission time.

Alternatively, the *measured* Ascension Doppler can be used to infer the *Cory Chouest* offset, as shown.

The agreement between the offsets measured locally by GPS and those inferred from Doppler measurements at a distance of 9200 km is remarkable. It demonstrates at once the reality of the GPS and the Doppler measurements. Differences are of the order of 10 m rms. These could be attributed to GPS errors or to motion of the acoustic-source array suspended at a depth of 175 m relative to the ship.

3. Offset spectra

The spectra in Fig. 2 refer to measurements taken on our way to Cape Town subsequent to the Heard Island transmissions. The plotted spectra refer to the components in ship coordinates: fore and aft (surge spectrum) and port–starboard (sway spectrum). The principal contribution to the offset spectra comes from the low frequencies. At the high frequencies, the surge component systematically predominates over the sway component, suggesting a navigational contribution above 60 cycles per hour.

We are not able to provide decisive information concerning the physical processes responsible for the offsets. One possibility is the effect of the variable wind and wave field. Another possibility is the effect of a variable surface flow superimposed on the ship's velocity vector $\mathbf{U}$. If this variable flow is of low temporal frequency, then the proper interpretation of the measured spectra is in terms of spatial frequency k, as shown on the right and top scales of Fig. 2. The conversion is accomplished by using $\omega = \mathbf{k} \cdot \mathbf{U}$, taking into account the ships speed.

4. Vorticity and divergence

Our first thought was that the offsets could be interpreted in terms of large-scale circulation features. Accordingly, we steamed along a zig-zag course with 2-h legs, and analyzed the offsets in terms of a prevailing vorticity and divergence. It would indeed be exciting if GPS navigation could provide a measure of open-sea vorticity and divergence (and hence, of the vertical circulation). The computed vorticity and divergence were both of the order of 10^{-5} s^{-1}. We learned, how-

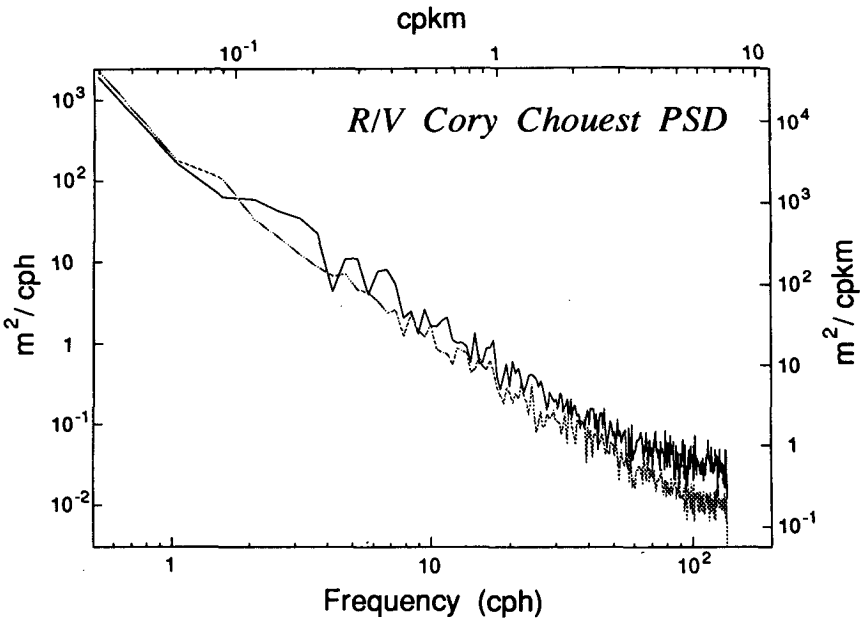

FIG. 2. Ensemble average of spectra from six 2-h records taken at 1200–2400 UTC 11 February 1991. Solid line refers to the along-track component of offsets, dashed line to the cross-track component. Scales on top and to the right correspond to a frozen field. The records were taken in the Indian Ocean on the way into Cape Town, on a zig-zag course with 2-h legs moving at 10 kt.

ever, that these quantities showed no persistence, varying in magnitude and sign from leg to leg. Our measurements were much too sparse to permit any conclusions, but as far as the measurements go, they do not seem to be associated with the large-scale circulation features.

5. Internal waves

Here the situation is different. The measured offsets are of a magnitude to be expected for typical internal-wave conditions. In fact, they are somewhat smaller than expected, and on hindsight, it would have been remarkable had such offsets not been observed. The characteristic internal-wave phase velocities are small as compared to the ship's speed, and the interpretation of the spectra is in terms of spatial wavenumbers rather than temporal frequencies.

The spectral shape is consistent with prevailing internal-wave models. This is demonstrated in a lengthy Appendix, which is included as we could not find any published reference to the required spectral projection: horizontal displacement component projected onto a single wavenumber component.

For frequencies ω well above the Brunt–Väisälä frequency N, the horizontal wavenumber is given by

$$k = \frac{j\pi}{b}\frac{(\omega^2 - f^2)^{1/2}}{N}, \qquad (2)$$

where $b \approx 1$ km is a stratification scale (Munk 1981), $f = 7.3 \times 10^{-5}$ s^{-1} is the Coriolis frequency, and j is the vertical mode number with a representative value $j^* = 3$. For the case $\omega^2 = 2f^2$ the numerical values yield a wavelength $2\pi/k = 31$ km, and a phase speed $\omega/k = 0.5$ m s^{-1}. The phase speed is small compared to the ship's speed of 5 m s^{-1} = 10 kt, and accordingly the measured frequency spectrum (in cycles per hour) can be regarded as a wavenumber spectrum (in cycles per 10 nautical miles).

We need to estimate the magnitude of the expected offsets. The ship is moving at a mean speed plus the surface orbital velocity of internal waves. For a Garrett–Munk (GM) isotropic internal-wave spectrum (Munk 1981), the component offset spectrum (either ξ or η) is found from

$$F_\xi(\omega, j) = \tfrac{1}{2}\omega^{-2}F_u(\omega, j)$$
$$= \pi^{-1}Eb^2N_0^2 f\omega^{-5}(\omega^2 + f^2)$$
$$\times(\omega^2 - f^2)^{-1/2}H(j).$$

$$\langle\xi^2\rangle = \langle\eta^2\rangle$$
$$= \sum_{j=1}^{\infty}\int_f^\infty F_\xi(\omega, j)d\omega = \frac{7}{16}Eb^2\left(\frac{N_0}{f}\right)^2, \qquad (3)$$

giving rms (ξ) = 370 m. Here $H(j)$ is the modal spectrum (see Appendix). But the measured offsets are relative to a 2-h mean (relative to a spatial mean averaged over $L = 37$ km), which implies a $1 - \mathrm{sinc}^2(\frac{1}{2}kL)$

high-pass filter. The important contributions to the mean-square offsets are from wavenumbers for which $\sin\frac{1}{2}kL > \pi$. The corresponding frequency is found from (2); for $j^* = 3$ this gives a lower limit $\omega = 1.94f$ in place of $\omega = f$, and reduces rms offsets from 370 to 75 m. The measured offsets are of this order. The computed estimate is sensitive to the choice of j, and thus very uncertain.

The spectrum shown in Fig. 2 varies roughly as k^{-2} between 0.05 and 5 cycles per kilometer. For a comparison with the internal-wave model, we need to transform the spectrum from ω, j space to k_1, k_2, j space and then integrate over k_2 and j. The procedure is cumbersome and uninteresting (Appendix). The result is

$$F_{\xi_1}(k_1) = \frac{7}{16} Eb^2 \left(\frac{N_0}{f}\right)^2 \frac{2}{\pi} \frac{k_*}{k_*^2 + k_1^2},$$

which is consistent with (3). The important conclusion is that the computed spectrum varies as k^{-2} for large horizontal wavenumbers. (Here, k_* is a horizontal wavenumber scale that is not readily related to the vertical-mode scale j_*.)

It is perhaps unfortunate that this class of wave motion should be known under the name of *internal* waves, suggesting that unlike surface waves they do not play a role in the motion of surface ships. Internal waves are internal in the sense that the largest *vertical* displacement takes place in the interior. Horizontal displacement is in fact a maximum at the surface boundary.

6. Concluding comments

The purpose of this note is to encourage further measurements to decide whether small-scale offsets from a steady ship's course are associated with the internal-wave field; indeed, whether such offsets have a geophysical interpretation.

Acknowledgments. We are indebted to ONR, NOAA, DOE, and NSF for supporting the Heard Island experiment. A special thanks is due to the two reviewers for pointing out numerous discrepancies. If the original version of this note sounded to them like something written on shipboard at the end of a long and bumpy ride—it was!

APPENDIX

Offset Spectrum

We refer to the GM internal-wave spectrum for guidance (see Munk 1981 for notation). Let $u_1 = d\xi_1/dt$ be the component of particle velocity in direction x_1. For horizontal isotropy, the displacement spectrum at the surface ($N = N_0$) is given by

$$F_{\xi_1}(\omega, j) = \omega^{-2} F_{u_1}(\omega, j)$$

$$= \pi^{-1} E\beta^2 H(j) f^{-1} \frac{\sigma^2 + 2}{\sigma(\sigma^2 + 1)^{5/2}}, \quad \text{(A1)}$$

where the "Coriolis frequency excess"

$$\sigma = (\omega^2 - f^2)^{1/2}/f \quad \text{(A2)}$$

is a convenient dimensionless frequency. Here

$$\beta = b\left(\frac{N_0}{f}\right), \quad H(j) = \frac{(j^2 + j_*^2)^{-1}}{\sum_{j=1}^{\infty} (j^2 + j_*^2)^{-1}},$$

$$\sum_{j=1}^{\infty} H(j) = 1. \quad \text{(A3)}$$

Equation (A1) can be transformed to

$$F_{\xi_1}(\sigma, j) = F_{\xi_1}(\omega, j) \frac{d\omega}{d\sigma}$$

$$= \pi^{-1} E\beta^2 H(j) g(\sigma),$$

$$g(\sigma) = (\sigma^2 + 2)(\sigma^2 + 1)^{-3}. \quad \text{(A4)}$$

The mean-square displacement can be given in closed form:

$$\langle \xi_1^2 \rangle = \sum_{j=1}^{\infty} \int_0^{\infty} d\sigma F_{\xi_1}(\sigma, j) = \frac{7}{16} E\beta^2. \quad \text{(A5)}$$

For comparison with observations, we require $F_{\xi_1}(k_1)$, where $k_1 = k_H \cos\theta$ is the x_1 component of horizontal wavenumber

$$k_H = \frac{\pi\sigma j}{\beta}. \quad \text{(A6)}$$

For the isotropic spectrum

$$F(k_H)dk_H = F(k_1, k_2)dk_1 dk_2 = F(k_1, k_2)k_H dk_H d\theta$$

$$= 2\pi F(k_1, k_2)k_H dk_H,$$

so that

$$F(k_1, k_2, j) = \frac{F(k_H)}{2\pi k_H}$$

$$= \frac{1}{2\pi^4} E\beta^4 j^{-2} H(j)\sigma^{-1} g(\sigma). \quad \text{(A7)}$$

We now go into k_1, θ, ϕ space, where θ is azimuth and ϕ is tilt. In terms of the three-dimensional wavenumber k, we have

$$k_1 = k\cos\phi\cos\theta, \quad k_2 = k\cos\phi\sin\theta, \quad k_3 = k\sin\phi.$$

The vertical wavenumber k_3 is closely related to the mode number j; at the surface $k_3 = \pi j/b$. We then have

$$k_2 = k_1 \tan\theta, \quad j = pk_1, \quad p = \pi^{-1} b \tan\phi/\cos\theta \quad \text{(A8)}$$

$$F(k_1, \theta, \phi) = F(k_1, k_2, j) \frac{\partial(k_2, j)}{\partial(\theta, \phi)}$$

$$= (\pi^{-1} b k_1^2 \sec^2\phi/\cos^3\theta) F(k_1, k_2, j)$$

$$= \frac{1}{2\pi^3} E \frac{\beta^4}{b} \frac{1}{\cos\theta \sin^2\phi} H(j) \frac{g(\sigma)}{\sigma} \quad \text{(A9)}$$

From (A3), $H(j) \approx 2\pi^{-1} j_*(j^2 + j_*^2)^{-1}$. Now using $j = pk_1$, $j_* = pk_*$,

$$F_{\xi_1}(k_1, \theta, \phi) = \frac{E}{\pi^3} \frac{\beta^4}{b^2} \frac{1}{\sin^2\phi \tan\phi} \frac{g(\sigma)}{\sigma} \frac{k_*}{k_*^2 + k_1^2}. \quad \text{(A10)}$$

It is convenient to make one further transformation, noting that

$$\sigma = \frac{\beta k_H}{\pi j} = \frac{N_0}{f} \cot\phi,$$

so that

$$F_{\xi_1}(k_1, \theta, \sigma) = F(k_1, \theta, \phi) d\phi/d\sigma$$

$$= \pi^{-3} E \beta^2 g(\sigma) \frac{k_*}{k_*^2 + k_1^2}. \quad \text{(A11)}$$

The one-dimensional spectrum is then given by

$$F_{\xi_1}(k_1) = \int_0^{2\pi} d\theta \int_0^{\infty} d\sigma F_{\xi_1}(k_1, \theta, \sigma).$$

In the GM internal-wave spectrum, $j^* = 3$ is taken as constant, and accordingly,

$$k_* = \frac{j_*}{p} = j_* \left(\frac{\pi}{b}\right)\left(\frac{f}{N_0}\right) \sigma \cos\theta$$

is a function of σ and θ in the above equation. This makes things complicated. But there is no good physical reason why either j_* or k_* should be taken as scaling constants. For the present purpose, it is much simpler to take k_* as constant, and perform the integration:

$$F_{\xi_1}(k_1) = \frac{7}{16} E\beta^2 \frac{2}{\pi} \frac{k_*}{k_*^2 + k_1^2}. \quad \text{(A12)}$$

For comparison with the measured spectrum (positive k_1 only), we confirm that

$$\langle \xi_1^2 \rangle = \int_0^{\infty} F_{\xi_1}(k_1) dk_1 = \frac{7}{16} E\beta^2, \quad \text{(A13)}$$

in agreement with Eq. (3) in the text.

Write

$$F_{\xi_1}(k_1) = \alpha \frac{2}{\pi} \frac{k_*}{k_*^2 + k_1^2},$$

$$\alpha = \frac{7}{16} E\beta^2 = 0.143 \text{ km}^2. \quad \text{(A14)}$$

The numerical value is for $E = 6.3 \times 10^{-5}$, $b = 1$ km, $N_0 = 3$ cph, $f = 1$ cpd $= 1/24$ cph (30° lat), $\beta = 72$ km.

We wish to compute $\langle \xi_1^2 \rangle$ as a function of cutoff wavenumber k_L:

$$\langle \xi_1^2 \rangle_{k_L} = \int_{k_L}^{\infty} F_{\xi_1}(k_1) dk_1 = \alpha\left(1 - \frac{2}{\pi} \tan^{-1} \frac{k_L}{k_*}\right)$$

$= \alpha$ for $k_L = 0$, hence, rms $(\xi_1) = 378$ m

$= 1/2\alpha$ for $k_L = k_*$,

hence, rms $(\xi_1) = 267$ m

$\approx 2\pi^{-1} \alpha k_*/k_L$ for $k_L \gg k_*$.

Here $k_L = 1/L$ and $L = 37$ km is the distance covered for each of the 2-h runs. Comparison with measured variances requires k_* of order 10^{-3} cycles per kilometer. For the 1-h run at 3 kt (Fig. 2), $L \approx 5$ km and the variances are accordingly much smaller.

REFERENCES

Metzger, K., Jr., 1983: Signal processing equipment and techniques for use in measuring ocean acoustic multipath structures. Ph.D. thesis, University of Michigan, Ann Arbor, MI, 316 pp.

Munk, W., 1981: Internal waves and small scale processes. *Evolution of Physical Oceanography*, B. A. Warren and C. Wunsch, Eds., MIT Press, 264–291.

——, and A. Forbes, 1989: Global ocean warming: An acoustic measure? *J. Phys. Oceanogr.*, **19**, 1765–1778.